AGU PUBLICATIONS

JGR

Journal of Geophysical Research: Atmospheres

RESEARCH ARTICLE

10.1002/2016JD026032

Key Points:
- Light absorption measurements were carried out at a high-altitude site in southeast Tibet
- Peaks in BC were coincident with deeper atmospheric boundary layers
- During pollution events BC DRF contributed to the total atmospheric forcing was significantly higher (~50%) than usual (~20%)

Supporting Information:
- Supporting Information S1

Correspondence to:
J. Cao,
cao@loess.llqg.ac.cn

Citation:
Zhao, Z., et al. (2017), Black carbon aerosol and its radiative impact at a high-altitude remote site on the southeastern Tibet Plateau, *J. Geophys. Res. Atmos.*, *122*, 5515–5530, doi:10.1002/2016JD026032.

Received 1 OCT 2016
Accepted 30 APR 2017
Accepted article online 3 MAY 2017
Published online 22 MAY 2017

Black carbon aerosol and its radiative impact at a high-altitude remote site on the southeastern Tibet Plateau

Zhuzi Zhao[1], Qiyuan Wang[1], Baiqing Xu[2], Zhenxing Shen[3], Rujin Huang[1], Chongshu Zhu[1], Xiaoli Su[1], Shuyu Zhao[1], Xin Long[1], Suixin Liu[1], and Junji Cao[1,4]

[1]Key Laboratory of Aerosol Chemistry and Physics, Institute of Earth Environment, Chinese Academy of Sciences, Xi'an, China, [2]Laboratory of Tibetan Environment Changes and Land Surface Processes, Institute of Tibetan Plateau, Chinese Academy of Science, Beijing, China, [3]Department of Environmental Science and Engineering, Xi'an Jiaotong University, Xi'an, China, [4]Institute of Global Environmental Change, Xi'an Jiaotong University, Xi'an, China

Abstract Aerosol black carbon (BC) was measured with an Aethalometer™ at Lulang, a high-altitude station in southeastern Tibetan Plateau (TP), from July 2008 to August 2009. Daily mean BC loadings varied from 57.7 to 5368.9 ng m^{-3} (grand average ± standard deviation = 496.5 ± 521.2 ng m^{-3}), indicating a significant BC burden even at free tropospheric altitudes. BC loadings were highest during the premonsoon and lowest during the monsoon, and peaks in BC were coincident with high atmospheric boundary layers. Daily peaks in BC occurred from 08:00 to 10:00 local time with minor fluctuations at other times. The BC mass absorption efficiency (MAE) was calculated from elemental carbon concentrations obtained from a thermal/optical reflectance method and absorption coefficients from the Aethalometer™, and values ranged from 6.1 to 31.7 m^2 g^{-1} (average = 16.6 ± 5.7 m^2 g^{-1}). Strong variations in the MAEs during the monsoon can be ascribed to large uncertainties due to low BC and b_{abs} and possibly coatings on the BC. High MAEs during premonsoon pollution events were likely due to internal mixing during transport. The mean direct surface radiative forcing (DRF) estimated from a radiation model was −19.9 (±7.4) W m^{-2} for the full aerosol population and −3.9 (±1.8) W m^{-2} for a BC only scenario. The BC DRF during a case study (−36.0 W m^{-2}) was much stronger than the typical, and the BC contribution to the forcing was higher (~50%) than usual (~20%). These results show that BC can at times account for a relatively large fraction of the aerosol surface heating over the southeast TP, which may affect both climate and hydrological cycles.

1. Introduction

Atmospheric aerosols influence the Earth's radiation budget through the scattering and absorption of both solar and terrestrial radiation [*Intergovernmental Panel on Climate Change*, 2013]. Black carbon (BC) aerosol, the dominant fraction of light-absorbing particles for visible wavelengths, is a byproduct of the incomplete combustion of fossil fuels and biomass [*Bond et al*., 2013]. This form of carbon is chemically inert and mostly exists in the submicron size (<1 μm) regime [*Babu and Moorthy*, 2002]. Under some conditions, aerosol BC can lead to warming in the lower atmosphere, and therefore, BC concentrations are a key variable in model calculations of aerosol optical properties and direct radiative forcing (DRF) over regional to global scales [*Haywood and Shine*, 1997]. As BC particles have lifetimes of a few days to weeks [*Bond et al*., 2013], they can be transported to long distances, even to remote locations such as the Arctic [*Stohl et al*., 2006], Antarctica [*Chaubey et al*., 2011; *Tomasi et al*., 2007], and the Himalayas [*Dumka et al*., 2010; *Hyvärinen et al*., 2009; *Marinoni et al*., 2010]. Moreover, both laboratory and field observations suggest that aging can change the optical properties of BC particles, enhancing the light absorption [*Guo et al*., 2016; *Jacobson*, 2001; *Khalizov et al*., 2013, 2009; *Peng et al*., 2016; *Zhang et al*., 2008].These potential effects, together with the large quantities of BC injected into the atmosphere globally, make it imperative to give proper attention to the concentrations and properties of BC in remote regions [*Raju et al*., 2016].

In recent years, the urbanization and industrialization of Asia have resulted in a rapid increase of BC emissions; e.g., South Asia is one of the world's BC hot spots [*Bond et al*., 2007]. *Kopacz et al*. [2011] showed that the Tibetan Plateau receives most BC from western and central China, as well as from India, Nepal, the Middle East, Pakistan, and other countries. These regions are close to the Tibetan Plateau with a large amount of BC emissions; it is essential to investigate the physical properties, sources, and transport of BC aerosol on the TP. The transport of BC from densely populated areas to the Himalayas could lead not only to substantial radiative forcing but also to changes in the monsoon circulation and hydrological cycles [*Venzac et al*., 2008]. For

example, the deposition of BC onto snow can modify its albedo [*Flanner et al*., 2009; *Jacobson*, 2004], and this could lead to the retreat of glaciers [*Kulkarni*, 2006] thereby raising the threat of water shortages for downstream regions [*Xu et al*., 2009]. Therefore, BC studies at high-altitude sites in the Himalayas and TP are particularly valuable because they will improve our understanding not only of the potential importance of the region in terms of climate effects but also the impacts on other Earth systems.

Several field experiments have been conducted to investigate the BC aerosol over the TP during the past several decades. Most of those studies have focused on the southern Himalayas, and, in general, they have shown that this part of the plateau can be affected by pollutants from South Asia [*Kopacz et al*., 2011; *Srivastava et al*., 2012]. Pollutants can be delivered both by uplift associated with the typical valley circulation and by advection during regional and long-range transport events [*Babu et al*., 2011; *Bonasoni et al*., 2008]. Studies of snow and ice of glaciers on the TP suggested that BC was most likely transported from southern Asia [*Ming et al*., 2009]. Indeed, there has been growing interest in gathering data on the aerosol mass and chemical composition for the hinterlands of the TP, and this information has been used to evaluate anthropogenic impacts and identify possible pollution sources [*Cong et al*., 2007; *Engling et al*., 2011; *Ming et al*., 2009; *Wang et al*., 2015; *Xu et al*., 2014; *Zhao et al*., 2013; *Zhu et al*., 2016]. Nonetheless, continuous BC data for extended periods of time and assessments of the BC contribution to the total aerosol DRF over many parts of the TP are still quite limited.

The main objectives of this study were to identify and evaluate the principal factors influencing BC variability and its optical properties over the southeastern TP. In addition, we were able to assess the contribution of BC aerosol to the DRF in the region by making simultaneous, colocated measurements of aerosol chemical composition. The study provides information that will be useful not only for characterizing tropospheric background conditions but also for improving the performance of climate and atmospheric chemistry models.

2. Materials and Methods

2.1. Site Description

Lulang is located on the western side of the Yarlung Tsangpo River in Linzhi Prefecture, which is on the southeastern part of the TP. The measurement site (94.44°E, 29.46°N, ~3300 m above sea level) was established as an integrated observation station for alpine research by the Chinese Academy of Sciences. There are extensive forests in the Linzhi region, and the sampling site was located in a remote area with no major anthropogenic sources nearby. Only several small villages were near the sampling site, and these were at distances of ~30 to 50 km. Further details on the site may be found in *Zhao et al*. [2013].

As a result of their altitude, the Himalayas act as a "physical wall" that impedes the outflow of pollutants from South Asia; however, the Yarlung Tsangpo River valley can be considered as a "leak in the wall." In fact, moisture can be transported from the Bay of Bengal, along the BrahmaPutra, Yarlung Tsangpo River northward into the northern TP and its tributaries toward to the west, and the resulting intrusions of moist air can eventually extend to the southeastern TP. This circulation pattern also allows contaminants emitted from southern Asia to be transported into the same region under some meteorological conditions [*Cao et al*., 2010]. Thus, our site in the southeastern part of the TP is an ideal location for studying transport of pollutants from South Asia.

2.2. Measurements of BC

The concentrations of BC were measured continuously from 19 July 2008 to 26 August 2009 using an Aethalometer™ (Magee Scientific, Model AE-16, Berkeley, CA) based on the optical transmittance at a single wavelength (λ = 880 nm). This instrument measures the light attenuation (ATN) transmitted through a quartz-fiber filter. Sample air was drawn through approximately ~2 m of conductive silicone tubing to the Aethalometer™ which was equipped with a total suspended particle inlet and operated at a flow rate of 4 L min^{-1}. The aerosol particles were dried with a silica gel dyer before entering the instrument to minimize the artifacts from water condensation. The ATN data from the Aethalometer™ are converted to BC mass by assuming a fixed BC specific attenuation cross section of 16.6 m^2 g^{-1} [*Virkkula et al*., 2007]. Details of the instrument's operating principles have been presented elsewhere [*Cao et al*., 2010, 2015; *Zhu et al*., 2016].

A potential limitation of the Aethelometer™ is that as the unit's filter tape advances, the BC concentrations can rise [*Arnott et al*., 1999; *Virkkula et al*., 2007], and therefore, the relationship between ATN and BC

concentration may not always be linear [*Weingartner et al*., 2003]. This "loading effect" must be taken into account by using empirical correction algorithms. In order to account for this artifact, two empirical factors (C and R(ATN)) are used for correcting the measured absorption due to the multiple scattering and shadowing effects, respectively [*Weingartner et al*., 2003]. The "real" aerosol absorption coefficient (b_{abs}) can be calculated as follows:

$$b_{abs} = \frac{\mathrm{ATN}}{C \cdot R(\mathrm{ATN})} \tag{1}$$

$$R(\mathrm{ATN}) = \left(\frac{1}{f} - 1\right) \frac{\ln(\mathrm{ATN}) - \ln(10\%)}{\ln(50\%) - \ln(10\%)} + 1 \tag{2}$$

Here we used C = 2.14 and f = 1.103 during wintertime and 1.114 for the other seasons following *Ram and Sarin* [2009]. As Lulang is a high-altitude site, the sample volume was corrected for standard temperature and pressure (see supporting information for details). The uncertainty in the BC mass concentration measurements is ~10% [*Ramachandran and Rajesh*, 2007; *Singh et al*., 2015].

2.3. Filter-Based Measurements

Along with the BC measurements, samples of total suspended particulates (TSPs) were collected using a medium-volume air sampler (Model KC-120H QingDao Laoshan Sampler, Laoshan Electronic Instrument Factroy Co., LTD., QingDao, China), which operated at an average flow rate of 40 L min^{-1}. Quartz-fiber filters (90 mm in diameter, QM-ATM, Whatman Ltd., Clifton, NJ, USA) were used as substrates for the collection of the TSP samples. Sampling was normally conducted once every 6 days starting at 10:30 local time, and sampling intervals were typically 3 days. Prior to sampling, the quartz-fiber filters were preheated at 900°C for 3 h to remove residual carbon. Field blank filters were also collected periodically to account for any artifacts introduced during the sample handling process, and the data were corrected using the average of these blanks. A total of 61 samples was obtained during the entire campaign period.

The TSP samples were equilibrated for 24 h at a temperature of 20–23°C and RH of 35–45% and then weighed on a Sartorius MC5 electronic microbalance with a sensitivity of ±1 μg (Sartorius, Göttingen, Germany). Each filter was weighed at least three times or until a stable reading was obtained, and the net mass accumulation was calculated by subtracting the difference between the averaged postsampling and presampling weights.

Organic carbon (OC) and elemental carbon (EC) were measured using a thermal/optical reflectance (TOR) method on a DRI Model 2001 Thermal/Optical Carbon Analyzer (Atmoslytic Inc., Calabasas, CA, USA). The IMPROVE_A protocol [*Chow et al*., 2007] produces four OC fractions (OC1, OC2, OC3, and OC4 at different temperatures in a 100% helium (He) atmosphere), a pyrolyzed carbon fraction (OP), and three EC fractions (EC1, EC2, and EC3 in a 98% He/2% O_2 atmosphere at different temperatures). OC was defined as OC1 + OC2 + OC3 + OC4 + OP and EC as EC1 + EC2 + EC3 − OP. A detailed description of the quality assurance/quality control (QA/QC) procedures can be found in *Cao et al*. [2003].

The concentrations of two water-soluble inorganic ions (SO_4^{2-} and NO_3^-) were determined with a Dionex-600 ion chromatography (Dionex Inc., Sunnyvale, CA, USA). The instrument was equipped with an IonPac AS14A column (8 mM Na_2CO_3/1 mM $NaHCO_3$ as the eluent) for anion analysis. The detection limits were 20 $\mu g L^{-1}$ for SO_4^{2-} and 15 $\mu g L^{-1}$ for NO_3^-. Standard reference materials produced by the National Research Center for Certified Reference Materials in China were analyzed for QA/QC purposes [*Zhang et al*., 2011]. Field blank levels were averaged and subtracted from the samples (0.304 μg mL^{-1} for SO_4^{2-} and 0.191 μg mL^{-1} for NO_3^-). Ten percent of the samples were submitted for replicate analyses, yielding coefficients of variance of ±1.39% for SO_4^{2-} and ±2.34% for NO_3^-.

Benzo[e]pyrene (BeP) and Benzo[a]pyrene (BaP) in polycyclic aromatic hydrocarbons (PAHs) were analyzed by thermal desorption gas chromatography-mass spectrometry (TD-GC-MS) with the use of an Agilent 7890A/5975C system. The electron ionization mass spectra (70 eV) were acquired over a mass range (m/z) of 30 to 570 amu, and the selected ion mode was used for quantification. PAHs were identified using both the retention time from the GC chromatograph and comparisons of the MS spectra with standards; the compounds were quantified with the use of an external standard. Details of the TD-GC-MS procedure have been described elsewhere [*Ho et al*., 2011]. A detailed description of the quality assurance/quality control (QA/QC) procedures can be found in *Chen et al*. [2014].

2.4. DRF Calculation

The DRF values at the local Earth's surface were estimated by a Tropospheric Ultraviolet and Visible (TUV) radiation model, which uses a total of 140 wavelength bands from 180 to 730 nm [*Madronich*, 1993]. Aerosol DRF is highly dependent on aerosol column burden and composition, which can be represented by aerosol optical depth (AOD), aerosol absorption optical depth (AAOD), single-scattering albedo (SSA), and asymmetric parameter (AP). Thus, AOD, AAOD, SSA, and AP were the key input parameters to the TUV model to estimate total aerosol DRF and BC DRF. In addition, surface albedo is another factor that influences the DRF, and it was derived from measurements made with the Moderate Resolution Imaging Spectroradiometer.

In this study, the AOD, AAOD, SSA, and AP data were retrieved from an Optical Properties of Aerosols and Clouds (OPAC) model [*Hess et al*., 1998] that used ground-based measurements as inputs. The OPAC model includes a data set of microphysical properties, and the aerosol optical properties can be calculated for different wavelengths and for different humidity conditions (e.g., 0, 50, 70, 80, 90, 95, 98, and 99%). This model consists of 10 major aerosol components, namely, insoluble, water soluble (including sulfate and nitrate), soot, mineral dust (coarse, accumulation, and nucleation), mineral transported, sea salts (coarse and accumulation), and sulfate droplets. Using different combinations of these aerosol components, 10 different aerosol types are defined, namely, (1) continental clean, (2) continental average, (3) continental polluted, (4) urban, (5) desert, (6) maritime clean, (7) maritime polluted, (8) maritime tropical, (9) Arctic, and (10) Antarctic. Each aerosol type is representative of a climatologically distinct environment. In each case, the data are given for 1 particle cm^{-3}, assuming that the particle is spherical and externally mixed.

For the model calculations, the measured aerosol mass concentrations were first converted into number concentrations, and because there were no measurements of particle size distributions, lognormal distributions were assumed and applied to each component *i* [*Hess et al*., 1998]:

$$\frac{dN_i(r)}{dr} = \frac{N_i}{\sqrt{2\pi} r \log\sigma_i \ln 10} \exp\left[\frac{1}{2}\left(\frac{\log r - \log r_{\mathrm{mod}N,i}}{\log\sigma_i}\right)^2\right] \tag{3}$$

where $r_{\mathrm{mod}N,i}$, σ_i, and N_i are the model radius, the width of the distribution, and the total particle number concentration of component *i*. The microphysical properties (e.g., $r_{\mathrm{mod}N,i}$, σ_i, and density of the particles) of aerosol components used here could be found in Table 1c in *Hess et al*. [1998]. Second, Mie theory was used to calculate the aerosol optical properties, including the extinction coefficient, scattering coefficient, and absorption coefficient; these were normalized to a number density of 1 particle cm^{-3}. To estimate the ambient values for these parameters, the normalized results were multiplied by the total particle number concentrations. Finally, the modeled extinction coefficient, absorption coefficient, and scattering coefficient were used to calculate the AOD, AAOD, and SSA on the base of exponential aerosol height profiles ($N(h)$), which is defined as follows [*Hess et al*., 1998]:

$$N(h) = N(0)e^{-\frac{h}{Z}} \tag{4}$$

where $N(0)$, h, and Z represent the number concentration of particles at the surface layer, the altitude above ground in kilometers, and the scale height in kilometers, respectively. Seasonal mixing layer heights for the station were adjusted using data downloaded from European Centre for Medium-Range Weather Forecasts (ECMWF).

In this study, the "continental average" aerosol type was selected as the starting point for modeling the aerosol components. The main components of this aerosol type include the water-insoluble and water-soluble fractions of the aerosol particles and BC. We fixed the number concentrations of water soluble, insoluble, and BC on the basis of the measured concentrations at the RH closet to the ambient RH values. Then, the number concentrations of other components, such as mineral dust in coarse and fine modes, were iteratively adjusted and constrained based on the observed BC mass fraction until the OPAC-derived AOD agreed with the satellite-derived AOD to within 5%. Although there is uncertainty in OPAC calculation by using chemical compositions, the OPAC model provides a chance to obtain the optical properties of aerosols on the basis of mass concentrations of chemical components [*Hess et al*., 1998]. And the OPAC method is well established and has been extensively used to derive crucial aerosol optical parameters for radiative forcing estimations at various locations [*Aruna et al*., 2016; *Raju et al*., 2016; *Srivastava et al*., 2012].

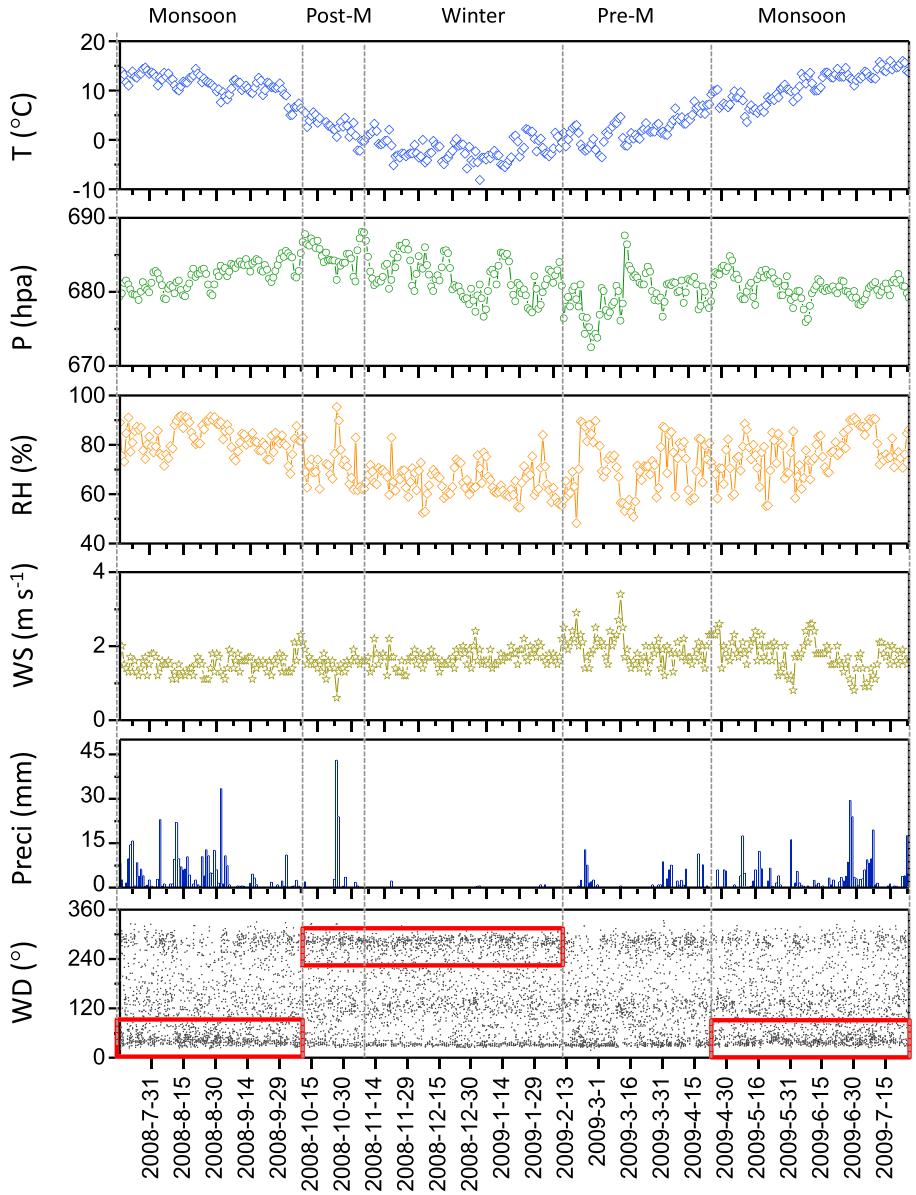

Figure 1. Temporal variations of temperature (*T*), pressure (*P*), wind speed (WS), relative humidity (RH), precipitation (Preci), and wind direction (WD) for the full sampling campaign.

In this way, the OPAC-derived optical properties (e.g., AOD, AAOD, and SSA) for the total aerosol and for BC particles alone were separately used as the original default values in the TUV model for Lulang. The DRF of total aerosols (or BC) at the surface was defined as the difference between the net shortwave radiative flux with and without aerosol as follows:

$$\mathrm{DRF}_{\mathrm{surface}} = \mathrm{Flux\ (net)}_{\mathrm{with\ aerosol\ (or\ BC),surface}} - \mathrm{Flux\ (net)}_{\mathrm{without\ aerosol(or\ BC),surface}} \quad (5)$$

2.5. Meteorological Conditions

As Lulang is a high-altitude mountain station, it is minimally affected by human activities, and therefore, information on the prevailing meteorology is especially important for understanding the aerosol characteristics. In general, the weather in this region is controlled by the Indian monsoon system in summer, which is characterized by relatively high temperatures and humidities and prevailing southerly winds. In the other parts of the year, westerlies dominate the large-scale atmospheric circulation, and there is limited precipitation. In

addition, during winter and spring, the southern branch of the westerlies sweeps over the southern side of the Himalaya-Hindu Kush range and impacts the southeastern TP [*Chen et al*., 2014; *Wang et al*., 2016]. In addition to the large-scale effects of the atmospheric circulation, local orographic effects on air pollutant transport also need to be taken into account [*Hindman and Upadhyay*, 2002]. In particular, in mountainous areas, temperature differences between mountaintops and lowlands often cause diurnal valley wind systems that blow upward during the day and reverses during the night.

Meteorological data were recorded from an 18 m tall atmospheric boundary layer tower; the measurements included wind speed, wind direction (034B, Met One), relative humidity, air temperature (GMP45C-GM, Campbell SCI), air pressure (PTB220A, Vaisala), and rain intensity. Temporal variations of all these parameters (temperature (T,°C), pressure (P,hPa), relative humidity (RH, %), precipitation (mm), wind speed (WS, m s^{-1}), and wind direction (WD, degrees measured clockwise from north)) over the course of our study are shown in Figure 1. As evident in that figure, the warmest month of the year was August, while the coldest was December. The ambient pressure showed very little variation, being the highest in October with a value of 684.8 ± 1.5 hPa and lowest in February (678.8 ± 3.2 hPa). Surface winds were the strongest during February and March and lowest during July and August. Precipitation at Lulang showed a rapid increase from March to June and then stayed at a high value until October (~120 mm per month averaged from June to September). It is worth noting that relatively high levels of RH and precipitation were found in Lulang compared with other high-altitude sites in the Himalayas or the TP [*Babu et al*., 2011; *Bonasoni et al*., 2008; *Wan et al*., 2015], and this indicates that the sampling site was influenced by a "moisture passage" effect.

As noted above, seasonal variations in atmospheric conditions are influenced by both the large-scale circulation patterns and the local mountain-valley breeze regime. The winds at the Lulang station showed a bidirectional distribution, with one dominant direction from the bottom of the valley (NE-E) and the other from the upper mountain (SW-W). For most of the year (October to May), mountain winds prevailed during nighttime, while valley winds prevailed during daytime. During the monsoon, valley breeze winds can predominant during nighttime due to the large-scale forcing [*Ueno et al*., 2008]. The abrupt changes in local circulation, WD, and precipitation were used to operationally define the monsoon phase over the study region and the other intervals as follows: premonsoon (18 February 2009 to 27 April 2009), monsoon (16 July 2008 to 3 October 2008 and 28 April 2009 to 26 August 2009), postmonsoon (4 October 2008 to 9 November 2008), and winter (10 November 2008 to 17 February 2009).

3. Results and Discussion

3.1. Characteristics of Surface BC Concentrations

3.1.1. Comparison of Optical and Thermal-Optical BC Measurements

A comparison between the correcting Aethalometer™ data versus TOR EC results was performed as a cross check on the methods, and the results are presented in Figure S1. Note that the BC concentrations, recorded every 5 min with the Aethalometer™, were integrated for periods of 120 h (similar to the total sampling time on the samples) to match the 61 EC samples. The simultaneous operation of the high-volume sampler and the Aethalometer™ ensured sampling of the same ambient air. A regression line that passed through origin of the plot yielded a slope 0.78, with $R = 0.75$. However, after exclusion of two outliers, a stronger relationship was found between the Aethalometer™ and TOR measurements, with a correlation coefficient of 0.83. The least squares regression line passing through the origin of the plot had a slope of 1.07, indicating that the concentrations were similar, and therefore, the two techniques produce results that were in very good agreement.

3.1.2. Temporal Variations

The variations in BC showed a clear seasonal pattern with low loadings of 319 ± 170 ng m^{-3} (arithmetic mean ± standard deviation) during the monsoon and high values in the premonsoon (985 ± 1221 ng m^{-3}). Day-to-day variations of BC were generally more subdued during the monsoon, postmonsoon, and winter compared with the premonsoon (Figure 2). These seasonal variations are similar to those reported for a high-altitude Himalaya station called the Nepal Climate Observatory-Pyramid [*Marinoni et al*., 2010]. The monthly average BC loadings at Lulang ranged from a high of 1600 ± 1746 ng m^{-3} in March 2009 to a low of 191 ± 224 ng m^{-3} in August 2008, an eightfold difference. The minimum values of BC remained more

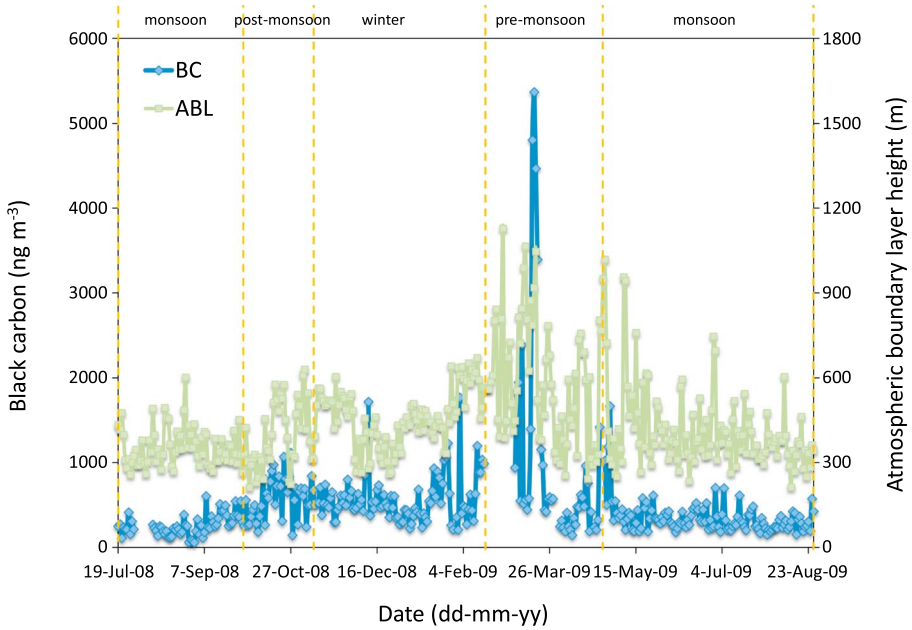

Figure 2. Temporal variations of the daily BC concentrations and atmospheric boundary layer (ABL) heights for the sampling campaign. (No data were acquired from 17 February to 5 March 2009 because of the failure of aethalometer.)

or less similar during all months, but the maximum values showed significant variations, with very high values during March.

The daily mean BC mass concentration averaged over the entire study was 497 ± 521 ng m^{-3}; a low of 58 ng m^{-3} occurred on 1 September 2008 and a high of 5369 ng m^{-3} on 17 March 2009. A frequency distribution plot of the hourly BC mass concentrations (Figure S2a) shows that the highest frequency occurred over a concentration range of 200–250 ng m^{-3}, which is 40–50% of the grand mean. Indeed, ~80% of the BC values were less than the annual mean BC loading, and this indicates a skew right distribution, that is, a tail of low frequencies at high concentrations. For example, the frequency for concentrations in the upper part of the distribution (>2000 ng m^{-3}), which accounted for only 3.0% of total data, was ~240 data points. In addition, the seasons with the maximum frequencies in a set of five arbitrarily defined bins of BC mass concentrations were as follows: ~57% monsoon (0–250 ng m^{-3}), 40% winter (250–500 ng m^{-3}), 23% postmonsoon (500–1000 ng m^{-3}), 11% premonsoon (1000–2000 ng m^{-3}), and 11% premonsoon (> 2000 ng m^{-3}) (Figure S2b). Seasonally, the largest fraction of BC mass occurred during the premonsoon; this seasonal average was 37%, 33%, and 22% higher than monsoon, postmonsoon, and winter, respectively, demonstrating that there was relatively more serious BC pollution over Lulang during the premonsoon.

The seasonal variability in BC mass concentration can best be understood in relation to regional meteorology, boundary layer dynamics, and variability in the sources. First, due to the dynamic transport by westerly winds in winter and the Indian monsoonal circulation in summer, the air quality in Lulang is at times impacted by the transport of the contaminants from heavily polluted regions. These circulation patterns allowed BC emitted from the vast sub-Himalayan and South Asia regions to be transported to the sampling facility [*Cao et al*., 2010]. Second, it is likely that a significant amount of the variability in the BC loadings is related to changes in the depth of the atmospheric boundary layer (ABL). As shown in Figure 2, we found that the major peaks of BC were always coincident with deeper ABLs. Moreover, an analysis of seasonal trends showed that the ABL was shallowest during the monsoon (384 ± 111 m), followed by postmonsoon (405 ± 119 m), and then winter (459 ± 99 m), and it was the deepest during the premonsoon (597 ± 223 m) when the BC loadings were the highest. In the premonsoon, the processes that led to the deep boundary layers also may have caused particles emitted from surrounding areas to become dispersed and mixed throughout the column, thus leading to relatively high BC levels. Relatively shallow ABL depths in other seasons decreased vertical mixing and suppressed the transport of aerosols from surrounding polluted areas, and that led to a decrease in the mass concentrations of various species.

Table 1. Concentrations of Black Carbon (BC) at Lulang Compared With Other High-Altitude Stations in the Tibetan Plateau and Himalayas and Selected Major Source Areas[a]

Sampling Site	Location	Longitude and Latitude	Altitude (m)	BC/EC Concentration (ng m^{-3})					Reference
				Premonsoon	Monsoon	Postmonsoon	Winter	Mean	
Lulang	Southeastern TP	29.46°N, 94.44°E	3,300	984.8	319.3	602.4	568	496.5	This Study
Ranwu	Southeastern TP	29.32°N, 96.96°E	4,600	139.1	/	/	413.2	276.15	*Wang et al.* [2016]
Beiluhe	Central TP	34.85°N, 92.94°E	4,600	621.6	/	/	204.8	413.2	*Wang et al.* [2016]
QOMS	Southern TP	28.36°N, 86.95°E	4,276	440	100	190	260	250	*Cong et al.* [2015]
Nam Co	Central TP	30.76°N, 90.98°E	4,718	200	150	110	340	190	*Wan et al.* [2015]
Qinghai Lake	Northeastern TP	36.97°N, 99.90°E	3,300	1,000	530	690	1,050	800	*Zhao et al.* [2015]
QSS station	Northeastern TP	39.50°N, 96.51°E	4,180	47	100	37	78	48	*Zhao et al.* [2012]
Hanle	Western part of trans-Himalayas	32.78°N, 78.96°	4,520	110	63	72	68	77	*Babu et al.* [2011]
NCO-P, Nepal	Himalayas	27.95°N, 86.82°E	5,079	320	56	137	125	159.5	*Marinoni et al.* [2010]
Muztagh Ata	Western TP	38.28°N, 75.02°E	4,500	/	163.7	164.2	96.5	133.1	*Zhu et al.* [2016]
Lasha	Central TP	29.65°N, 91.03°E	3,642	2,533.3	2,000	3,600	4,600	3,000	*Gao et al.* [2007]
Mukteshwar	Northwestern India	29.43°N, 79.61°E	2,180	1,216	532	692	786	806.5	*Hyvärinen et al.* [2009]
Monora Peak	Northwestern India	29.4°N, 79.5°E	1,950	1,600	620	1,400	1,633.3	1,150	*Ram et al.* [2010]
Mount Abu	Western India	24.6°N, 72.7°E	1,680	/	150	700	800	500	*Ram et al.* [2008]
Godavaril	Foothills of the Himalayas, Nepal	27.59°N, 85.31°E	1,600	1,826.7	502	480	1,105	930	*Stone et al.* [2010]
Sinhagad Pune (urban)	Western of India	18.35°N, 73.75°E	1,450	2,730	1,260	4,850	6,290	3,580	*Safai et al.* [2013]
Dhaka (Urban)	Bangladesh	23.76°N, 90.39°E		25,350	13,040	30,150	34,600	22,000	*Begum et al.* [2012]
Delhi (Urban)	India	28.58°N, 77.20°E	260	12,470	24,870	22,000	12,400	17,935	*Rai et al.* [2002]

[a]Note that different sampling cutoffs were used in the various studies.

Therefore, we conclude that the high premonsoon BC values observed at Lulang were influenced by the dynamics of the regional ABL because under some conditions regional pollution evidently was transported up to the high-altitude station. In combination with this, we note that substantial amounts of pollutants are emitted into the atmosphere during the dry season in South and Southeast Asia as a result of natural forest fires and human-initiated burning activities, most notably the burning of agricultural residues [*Gadde et al.*, 2009; *Sheesley et al.*, 2003; *Streets et al.*, 2003]. Likewise, simulation research has also indicated that sources in east India have a strong impact on BC contamination over the southeastern part of the TP [*Cao et al.*, 2010]. This seasonality in the BC emissions can contribute to high loadings, but the impact is greatest in the premonsoon. Above all, changes in source emissions during the premonsoon in concert with favorable meteorological conditions can lead to the transport of BC from the moderately populated but vast sub-Himalayan and South Asia regions to higher altitudes. This transport may be more efficient during March than other parts of the premonsoon and the monsoon because the washout of aerosols may become significant during the latter (Figure 1).

3.1.3. Comparisons With Other Stations

A comparison of the BC or EC measured at different locations is given in Table 1. The concentrations of BC in the Himalayas apparently decrease sharply with altitude; for example, BC concentrations measured at Lulang

were significantly higher than the values reported from Nam Co [*Ming et al*., 2010], QSS station [*Zhao et al*., 2012], Hanle [*Babu et al*., 2011], NCO-P [*Marinoni et al*., 2010], and Muztagh Ata [*Zhu et al*., 2016]. However, the concentrations of BC in urban sites located within high-altitude basins, as in Lhasa [*Gao et al*., 2007], can be 5 times higher than that in Lulang. Table 1 also shows the results of the measurements performed at other sites in the Nepal, Bangladesh, and the Indian subcontinent, which are major source areas for the aerosol transported to southeastern TP. Interestingly, the concentrations at mountain sites in India, despite their lower altitudes, are not significantly higher than in Lulang, suggesting that much of the southeastern sector of the TP is strongly influenced by pollution sources upwind. Not surprisingly, the BC concentrations at the urban stations, Dhaka [*Begum et al*., 2012], Delhi [*Rai et al*., 2002], and Sinhagad Pune [*Safai et al*., 2013], were significantly higher than the values at Lulang in all seasons. However, these stations showed a distinct seasonality in BC, with higher concentrations in the postmonsoon and winter compared with lower loadings in the premonsoon and monsoon. With reference to physical processes, the shallow ABL over the Indian mainland during winter [*Beegum et al*., 2009; *Gogoi et al*., 2009; *Nair et al*., 2007] results in a vertical confinement of species which contributes to the high BC concentrations over these stations during autumn/winter along with the high emissions. In contrast, during spring and summer, there is significant vertical dispersion of aerosols from the surface to the free troposphere due to increased thermal convection. This, in turn, leads to a displacement of BC from boundary layer to free troposphere where it is more susceptible to transport by synoptic winds. These factors also may be contributing to some of the observed seasonality at Lulang, especially the premonsoon high BC loadings.

3.1.4. Diurnal Variations and Seasonality

Obtaining information on the diurnal and seasonal variability of the BC aerosol contributes to our understanding of how mesoscale atmospheric processes and atmospheric boundary layer dynamics affect air pollution. The intraseasonal diurnal variability in BC mass concentrations and ABL heights during the study period over Lulang is plotted in Figure 3, which shows significant peaks in BC concentrations from 08:00 to 10:00 local time (LT) during all the seasons and minor fluctuations at other times of the day and night. As shown in Figure 3, the BC peaks occurred when the boundary layer developed, and this implies that boundary layer dynamics are an important determinant of how BC and other pollutants are transported to the sampling site. Over the mainland, as the ABL evolves after sunrise, strengthening thermals lift and eventually break the nighttime inversion causing the aerosols in the residual layer to mix with those near the surface leading to a sharp increase in the near-surface concentrations, an effect known as fumigation [*Stull*, 1988]. Later in the morning, solar heating induces valley winds which strengthen the mixing and dispersion of the aerosol, causing a significant dilution of BC near the site. Wind speeds also increase with solar heating, and they are highest around 13:00–15:00 (figure not shown), further facilitating dispersion and dilution of the aerosol—this can explain the low BC loadings in the afternoon. During the evening and throughout the night, surface temperatures decrease rapidly due to radiative cooling, which also results in weakening and thinning of the local boundary layer. The BC concentrations remained relatively stable from the afternoon through the night before reaching a minimum before sunrise, and this supports our contention that there were relatively low BC emissions at the sampling site.

Although there were relatively high BC levels over the entire day during the premonsoon, the morning peak was the highest in winter (1451 ng m^{-3}) and decreased in order from the postmonsoon (1302 ng m^{-3}) to the premonsoon (1238 ng m^{-3}) and finally the monsoon (360 ng m^{-3}). The comparatively small BC increase in the morning during the monsoon may be related to the limited local anthropogenic emissions. The higher variability of BC loadings during winter and the postmonsoon can be attributed to increased residential wood/biomass burning for heating in the surrounding villages in those seasons. However, since the limited population in the vicinity of the sampling site as well as no industrial operations or heavy motor vehicle traffic nearby, emissions from residential activities in surrounding villages may not led to the large BC enhancement between 08:00 and 10:00 during the winter, premonsoon, and postmonsoon. Hence, one possible explanation is the influences from regional transport. As shown in Figure 3, the BC peaks occurred as the boundary layer developed, and this implies that boundary layer dynamics are an important determinant of how BC and other pollutants are transported to the sampling site.

To investigate this potential effect, we examined several typical BC episodes as case studies. Figure S3a shows true color images of haze clouds from 16 to 18 March 2009 obtained with sensors aboard the

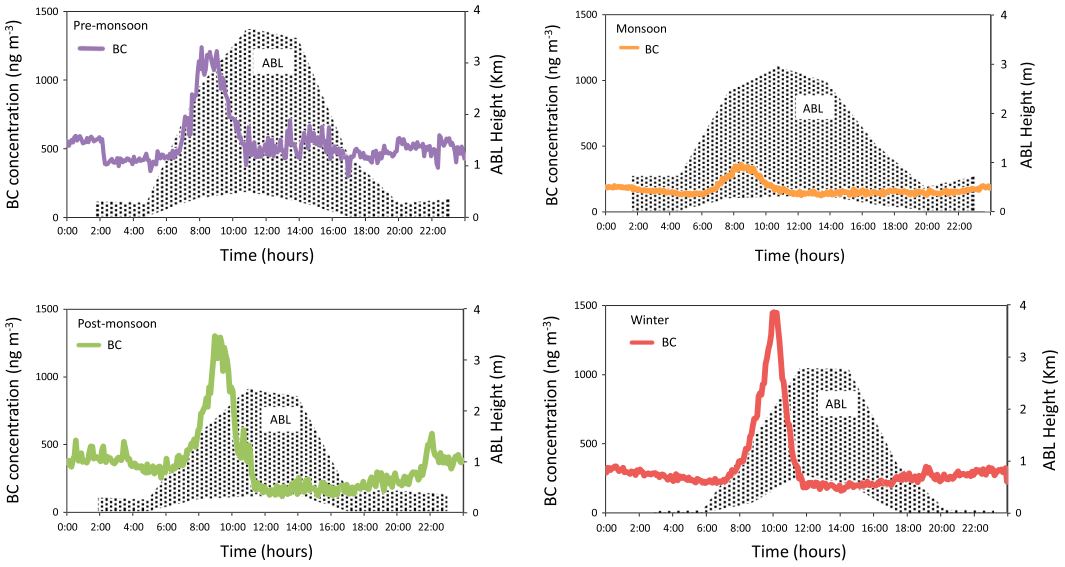

Figure 3. Diurnal variations of seasonal mean BC mass concentrations along with minimum and maximum atmospheric boundary layer heights (shown as shaded areas) over Lulang, (a) premonsoon, (b), monsoon (c), postmonsoon, and (d) winter. See text for definitions of seasons.

Terra Moderate Resolution Imaging Spectroradiometer (MODIS) satellite. Examination of the MODIS images shows a thick, widespread band of haze that was transported from the Bay of Bengal and piled up against the Himalayas in the late morning on each of these 3 days. Air mass back trajectory analysis was used to identify transport pathways for air pollutants, and the trajectories showed a flow pattern in which air masses under the control of the southern branch of westerlies passed over densely populated areas of the Indo-Gangetic Plain and Bangladesh and brought air pollutants from these regions to Lulang (Figure S3b). Further analyses of the event were made using the European Centre for Medium-Range Weather Forecasts (ECMWF) wind trajectories as shown in Figure S3c, and these analyses showed that the wind direction at ~07:00 in the vicinity of the measurement site was from the northeast to southwest for all 3 days. After sunrise, as solar heating commenced, the pollutants were advected by thermal winds and reached the northeastern slopes of the Himalayas (indicative of the pollution vertical extension in the MODIS images). Meanwhile, the wind direction at the surface shifted to the southeast at ~10:00, and that change allowed BC particles to be transported from the heavily polluted regions to the sampling site. *Xia et al.* [2011] also monitored a pollution episode at the Namco site in the central TP from 14 to 19 March 2009, and their results, consistent with ours, indicated that during that time, air pollution from upwind sources was transported to at least as far as the central TP.

3.2. Temporal Variability of Optical Parameters

The measurement of BC mass concentration via optical methods is relatively convenient and rapid but requires knowledge of "site-specific" mass absorption efficiency (MAE) [Ram and Sarin, 2009]. Various values for MAE (2–25 m2 g–1) have been reported, obtained based on independent and simultaneous measurements of EC concentration (by thermal method) and absorption coefficient (babs) by optical methods. Here we used the correcting AethalometerTM babs dividing by the TOR EC mass concentrations to derive the MAEs and further discussed the potential impacts of chemical species on MAEs. The corrected b_{abs} at $\lambda = 880$ nm derived from Aethalometer™ ranged from 1.3 to 65.3 M m^{-1} and averaged 8.2 M m^{-1} over the entire campaign period, and b_{abs} showed high values in the premonsoon months and low values in the monsoon. The calculated MAEs ranged from 6.1 to 31.7 m^2 g^{-1} with a higher average value of 18.2 m^2 g^{-1} in the monsoon compared with the other periods (15.8 m^2 g^{-1} for premonsoon, 14.3 m^2 g^{-1} for postmonsoon, and 15.6 m^2 g^{-1} for winter). Nonparametric tests (Kruskal-Wallis test) of the MAEs showed that overall test does not show significant differences (asymptotic significance level is 0.104, which is considered as a remarkable difference <0.05) across samples in different seasons. It should be noted in Figure S4 that several large MAE values (e.g.,

$>25\ m^2\ g^{-1}$, marked by circles) always corresponded to extremely low BC concentrations and b_{abs}, which may have led to large uncertainties in the calculations. However, in contrast, the highest MAE values (marked by red arrows) in the premonsoon coincided with high loadings of BC and other aerosol species (OC, sulfate, and nitrate) [*Zhao et al*., 2013].

Large variability in the MAE values has been reported and linked to different measurements, differences in location, particle composition, and the mixing state of BC in aerosols. For example, *Ram and Sarin* [2009] reported that the long-term average MAE at Monora Peak, India, from February 2005 to June 2007 was $12.8 \pm 2.9\ m^2\ g^{-1}$, while the MAE was observed to be somewhat lower in urban sites, such as Beijing (~9.4 [*Cheng et al*., 2011]) and Toronto (~5.5 [*Knox et al*., 2009]). Filter-based methods for the determination of MAEs depend on aerosol-filter interactions, that is, shadowing of the incident light with increasing filter loading and aerosol scattering effects [*Petzold et al*., 2005; *Arnott et al*., 2003], and a potential complication in these determinations is the influence of the aerosols' mixing state [*Bond et al*., 2006; *Schnaiter et al*., 2003; *Schnaiter et al*., 2005]. Indeed, BC aggregates are rarely emitted as pure BC, but typically are encapsulated, or "mixed" with other aerosol species [*Knox et al*., 2009]. When BC is internally mixed with other components such as sulfate and organic carbon, the coatings can focus light into the BC core of the particle, causing increases in the MAE values [*Liu et al*., 2015]. The relatively high MAE values observed at Lulang may be related to the BC mixing state because the particles have to travel for relatively long periods before reaching the remote site, and therefore, there are ample opportunities for coatings to accumulate on them [*Shiraiwa et al*., 2007]. Actually, diagnostic ratio of BeP/BaP in PAHs could generally give an indication of the aerosol age (>1.0 for aged aerosol) [*Oliveira et al*., 2011]. Both compounds are normally emitted in similar amounts by petrogenic sources, while BaP is more reactive than BeP. BeP/BaP ratio in Lulang is 1.71 ± 0.33 (min-max: 1.11-2.74) over the course of the study, supporting the contention of relatively aged aerosol in the sampling site.

As the filter-based measurements of BC do not provide information on the mixing state of the BC particles, we investigated the relationships between the concentrations of chemical species and MAEs by plotting the MAEs against several aerosol mass ratios EC/[NO_3^-], EC/[SO_4^{2-}], and EC/[OC] (Figure S5). High average values for the MAEs (19.7, 19.1, and $19.9\ m^2\ g^{-1}$) were observed when the ratios of EC/[NO_3^-], EC/[SO_4^{2-}], and EC/[OC] were <2.0, 0.4, and 0.1, respectively. However, the distribution of the MAEs was quite variable in this range, especially in the monsoon and premonsoon seasons. On the other hand, when the EC/[NO_3^-] (>2.5), EC/[SO_4^{2-}] (>1.0), and EC/[OC] (>0.1) ratios were high, the MAEs were relatively low and stable, with values around $15\ m^2\ g^{-1}$, and most of the MAEs in this range were observed in the winter and postmonsoon. Table 2 shows the seasonally averaged values of the EC and BC mass concentrations, attenuation coefficients, MAEs, and loadings of selected aerosol species (organic carbon, nitrate, and sulfate) at Lulang. Note that after excluding the outliers in the premonsoon (marked by red circles in Figure S5), only modest differences in the concentrations of OC, SO_4^{2-}, and NO_3^- were found among different seasons. The low levels of BC but higher OC at Lulang during the monsoon led to relative low EC/[OC] ratios (0.07 ± 0.03). The formation of secondary organic carbon is favored during the monsoon by the strong radiative flux at that time, combined with the high temperatures and RHs: these conditions may have favored the formation of coatings on the BC. As noted above, the calculations of MAEs during monsoon were likely affected by the uncertainties in the extremely low BC concentrations and b_{abs} values, but the possible presence of organic coatings on the BC particles also may have contributed to the uncertainties and variance in MAEs relative to other seasons.

During several unusual episodes in the premonsoon, atypically high concentrations of OC, SO_4^{2-}, NO_3^-, and BC (e.g., 11.4, 5.3, 1.4, and 3.0 $\mu g\ m^{-3}$) were observed, and these led to low EC/[NO_3^-] and EC/[SO_4^{2-}] ratios (1.68 ± 1.00 and 0.33 ± 0.00, respectively). The MAEs during these episodes reached $27.9\ m^2\ g^{-1}$, and as has been shown previously [*Zhao et al*., 2013], these high-aerosol episodes can be explained by the long-range transport of materials from upwind sources (e.g., eastern India and Bangladesh). The high MAE values also may have been a consequence of internal mixing during long-range transport which would have been favored by the abundant sulfate and nitrate. This process is important within the context of climate because as discussed above, mixing can change the optical properties—and therefore the radiative forcing of the aerosol—as the particles age.

Table 2. Seasonally Averaged Black Carbon (BC) and Elemental Carbon (EC) Mass Concentrations, Attenuation Coefficients, Mass Absorption Efficiencies (MAE), and Selected Chemical Components at Lulang

Parameter	Premonsoon	Monsoon	Postmonsoon	Winter	Annual	Premonsoon Excluding Episodes	Episodes[a]
$b_{abs\text{-}Aeth}$ (M m^{-1})	16.3 ± 20.3	5.3 ± 2.8	10.0 ± 4.1	9.4 ± 4.6	8.2 ± 8.7	9.1 ± 5.8	49.1 ± 22.9
BC (ng m^{-3})	984.8 ± 1220.5	319.3 ± 170.4	602.4 ± 246.9	568.0 ± 275.2	496.5 ± 521.2	547.0 ± 350.2	2956.3 ± 1377.8
EC (ng m^{-3})	837.2 ± 546.0	313.8 ± 173.3	671.9 ± 246.3	582.0 ± 161.0	536.1 ± 346.6	657.7 ± 308.5	1734.8 ± 699.1
MAE (m^2 g^{-1})[b]	15.8 ± 7.3	18.2 ± 5.9	14.3 ± 2.3	15.6 ± 5.1	16.6 ± 5.7	12.8 ± 3.8	27.9 ± 1.9
(min-max)	(6.1–29.3)	(10.1–31.7)	(10.3–16.6)	(7.1–28.0)	(6.1–31.7)	(6.1–19.6)	(26.5–29.3)
OC (μg m^{-3})	5.15 ± 3.89	4.27 ± 1.23	4.30 ± 1.61	3.65 ± 1.07	4.28 ± 2.05	3.91 ± 1.48	11.37 ± 7.36
NO_3^- (μg m^{-3})	0.45 ± 0.60	0.15 ± 0.07	0.17 ± 0.06	0.13 ± 0.06	0.21 ± 0.30	0.26 ± 0.14	1.40 ± 1.25
SO_4^{2-} (μg m^{-3})	2.07 ± 1.82	0.79 ± 0.99	0.75 ± 0.33	0.92 ± 0.55	1.07 ± 1.17	1.44 ± 0.91	5.26 ± 2.19
EC/OC	0.17 ± 0.04	0.07 ± 0.03	0.16 ± 0.05	0.17 ± 0.04	0.13 ± 0.06	0.17 ± 0.04	0.34 ± 0.05
EC/NO_3^-	2.75 ± 1.38	2.63 ± 1.93	4.00 ± 1.23	5.20 ± 2.00	3.50 ± 2.06	2.96 ± 1.52	1.68 ± 1.00
EC/SO_4^{2-}	0.50 ± 0.22	0.72 ± 0.74	1.00 ± 0.44	0.79 ± 0.43	0.72 ± 0.56	0.54 ± 0.24	0.33 ± 0.00

[a]Episodes: 5 to 8 march, 17 to 20 march; coincided with the points marked by red arrows in Figure S4.
[b]MAE was calculated by dividing the b_{abs} measured with the aethalometer by the EC mass concentrations from the TOR method.

3.3. Aerosol and BC Direct Radiative Forcing at Lulang

Aerosol radiative forcing is defined as the perturbation of the Earth atmosphere system due to the scattering and absorption of radiant energy by aerosols. Here the direct radiative forcing (DRF) was estimated at surface using the TUV model for two conditions: (1) the total aerosol condition and (2) the BC only condition. Seasonal values for the surface radiative forcing estimated for the composite aerosol populations are shown in Figure S6 where a net cooling effect is implied when the difference between the incoming solar radiation energy and outgoing thermal radiation is negative. The estimated mean surface forcing was −19.9 (±7.4) W m^{-2} for composite aerosols when averaged over the entire period. Earlier studies have reported that the mean surface forcings were −14.0 (±9.7) W m^{-2} and −18.9 W m^{-2} over Manora Peak (~2000 m), India [*Srivastava et al*., 2012], and the Himalayan Mohal Region (~1154 m) [*Guleria et al*., 2014; *Srivastava et al*., 2012], respectively, and these are comparable to the results from our study.

Relatively high surface forcing was observed during the premonsoon (−30.2 W m^{-2}) compared to other seasons (−12.8, −16.9, and −19.5 W m^{-2} for monsoon, postmonsoon, and winter, respectively), indicating stronger reductions in surface-reaching radiation during the premonsoon. We chose the surface DRF during one pollution episode during the premonsoon (17 to 20 March) for a comparison with more typical periods, and that case study showed that the total aerosol DRF during the episode (−74.3 W m^{-2}) was much stronger than during the monsoon. This difference of more than fivefold is an obvious consequence of the much larger aerosol mass loadings during the pollution episode (94.2 μg m^{-3}) compared with monsoon period (14.8 μg m^{-3}), and this analysis clearly shows that pollution events can lead to a reduction in surface-reaching radiation as a result of light scattering and absorption by the aerosol.

Figure S6 also shows the mean values for clear-sky BC DRF at the surface for the entire campaign as well as for the different seasons and selected episodes. The BC DRF during the study was −3.9 ± 1.8 W m^{-2}, and that contributed ~19.7 ± 7.6% of total aerosol surface DRF, but in comparison, BC contributed proportionately much less to the total aerosol mass loadings, only ~2.5%, during the study. Further comparisons show that the ~20% contribution of BC to the total aerosol DRF was lower than that (~50%) at Manora Peak [*Srivastava et al*., 2012], indicating that scattering by aerosol particles other than BC also was important at our site. Nevertheless, for the case study, the BC DRF (−36.0 W m^{-2}) was found to be much stronger compared with the premonsoon, monsoon, postmonsoon, and winter (−5.2, −1.3, −4.8, and −4.4 W m^{-2}, respectively). Previous studies have estimated the total aerosol surface forcing for both small-scale regional and large-scale pollution events at the NCO-P site, and the values ranged from −4 to −20 W m^{-2} [*Marcq et al*., 2010], which are somewhat lower than what we found for Lulang.

It is particularly noteworthy that the contribution of BC to the total aerosol DRF was 48.5% during the case study, which is about 2 to 4 times higher than the typical results for the various seasons. The observed increase in BC during the episode (6 times higher than the annual average concentration) would cause an increase in the absorption of solar radiation, a decrease in the amount of radiation reaching the surface, and warming of the atmospheric surface layer. Furthermore, as discussed in section 3.2, aging and chemical processing during transport would lead to internal mixing of BC, thus increasing the MAE through

enhancement in the absorption signal relative to the same amount of unmixed or externally mixed BC. Our study thus shows that the amount of radiation received at the surface is impacted by the presence of aerosol particles even at our remote, high-altitude station.

An analysis by *Bond et al.* [2007] showed that there are high emissions of BC over a broad swath of southern Asia. It is possible, if not likely, that the increase of BC in spring and summer (when solar radiation is abundant at these altitudes) would cause warming of the atmosphere due to absorption by these aerosol particles, and the advection of warm air from Southeast Asia over the Himalayan region would add to this effect [*Meehl et al.*, 2008; *Ramanathan et al.*, 2007]. Our studies demonstrate that surface radiative forcing during a pollution event in Lulang was both qualitatively and quantitatively different compared with more typical conditions, and that BC contributed roughly half to the total aerosol forcing during the event, which is much more than normal. This analysis shows that BC can at times account for a relatively large fraction of the surface heating effect caused by the aerosol population over the southeast TP region. The relatively high abundance of BC we found also has implications for snow melting both through its deposition onto snow surfaces and through dynamical coupling between land and atmosphere systems [*Lau et al.*, 2010].

4. Summary and Conclusions

High-altitude, remote regions of the Himalayas are often viewed as pristine environments, but at the same time they may be especially sensitive climate change and important for climate processes. For example, BC aerosols can heat the midtroposphere by absorbing solar radiation, and after deposition onto snow surfaces, the particles can enhance snow melting in the Himalayan regions and in this way affect both radiative fluxes and hydrological cycles. Our 1 year study was conducted in Lulang to characterize the principal factors that influence variability and optical properties BC over the southeast TP. This study has focused on BC and aerosol forcing at surface of the region, and we have shown some impacts of aerosol pollutants through coordinated measurements of aerosol optical properties, BC mass concentrations, and aerosol chemical composition. Major results are summarized below.

During the study period, the mean concentration of BC was 496.5 ± 521.2 ng m^{-3}, and the loadings varied over a range of 57.7–5368.6 ng m^{-3}. BC showed well-defined annual cycles, with a maximum during the premonsoon (984.8 ± 1220.5 ng m^{-3}), followed by the postmonsoon (602.4 ± 246.9 ng m^{-3}), winter (568.0 ± 275.2 ng m^{-3}), and a minimum during the monsoon (319.3 ± 170.4 ng m^{-3}). There was a major peak in BC in the morning from 08:00 to 10:00 local time (LT) during all the seasons, and there were minor fluctuations in BC concentrations throughout the rest of the day and night. Both the seasonal and diurnal variability in BC mass concentrations can be understood in terms of regional meteorology, boundary layer dynamics, and variability in the source strengths.

The b_{abs} at λ = 880 nm derived from an Aethalometer™ ranged from 1.33 to 65.25 M m^{-1} over the entire campaign period, averaged 8.2 M m^{-1}, and showed high values in the premonsoon months and low values in the monsoon. The calculated MAE ranged from 6.1 to 31.7 m^2 g^{-1} with an average value of 16.6 ± 5.7 m^2 g^{-1}. More variability in the MAEs was observed in monsoon compared to other seasons, and this can be ascribed to large uncertainties in MAE calculations caused by extremely low BC concentrations and b_{abs}, as well as possible effects resulting from organic coatings on the particles. Moreover, high MAEs during several premonsoon episodes could be explained by internal mixing during long-range transport, especially when sulfate and nitrate and their precursors were abundant.

The mean surface radiative forcing averaged over the entire study period was −19.9 (±7.4) W m^{-2} for the full aerosol population scenario. The DRF for the BC aerosol alone condition was −3.9 ± 1.8 W m^{-2}, which is ~20% of the total aerosol surface DRF. For the case study of a pollution episode, the BC DRF (−36.0 W m^{-2}) was found to be much higher compared with the premonsoon, monsoon, postmonsoon, and winter periods when the respective DRF values were −5.2, −1.3, −4.8, and −4.4 W m^{-2}. Moreover, the contribution of the BC fraction to the total aerosol DRF during episode was 48.5%, which is about 2 to 4 times higher than at other times. The results from this study provide valuable insights into optical characteristics of BC particles in the middle troposphere over a remote region, and they demonstrate potentially crucial impacts of BC and aerosol DRF over the southeast TP. The data also should be useful for modeling studies of the long-range transport of pollution and climate change.

Acknowledgments

This study was supported by the National Natural Science Foundation of China (41230641 and 41603129) and the General Financial Grant from the China Postdoctoral Science Foundation (2016 M592852). The authors are grateful to the Integrated Observation and Research Station for Alpine Environment in South-East Tibet, Chinese Academy of Sciences, for their assistance with field sampling. We are especially pleased to thank Haiqing Xu and Yongjie Wang for their kind help in the aerosol sampling and meteorological data analyses and three anonymous reviewers for their helpful comments on the manuscript. Data used in this study are available upon request from corresponding author at cao@loess.llqg.ac.cn.

References

Arnott, W. P., H. Moosmüller, C. F. Rogers, T. F. Jin, and R. Bruch (1999), Photoacoustic spectrometer for measuring light absorption by aerosol: Instrument description, *Atmos. Environ.*, *33*(17), 2845–2852, doi:10.1016/S1352-2310(98)00361-6.

Arnott, W. P., H. Moosmüller, P. J. Sheridan, J. A. Orgen, R. Raspet, W. V. Slaton, J. L. Hand, S. M. Kreidenweis, and J. L. Collett Jr. (2003), Photoacoustic and filter-based ambient aerosol light absorption measurements: Instrument comparisons and the role of relative humidity, *J. Geophys. Res.*, *18*(D1), 4034, doi:10.1029/2002JD002165.

Aruna, K., T. V. Lakshmi Kumar, B. V. Krishna Murthy, S. S. Babu, M. V. Ratnam, and D. N. Rao (2016), Short wave Aerosol Radiative Forcing estimates over a semi urban coastal environment in south-east India and validation with surface flux measurements, *Atmos. Environ.*, *125*, 418–428, doi:10.1016/j.atmosenv.2015.08.085.

Babu, S. S., et al. (2011), High altitude (~4520 m amsl) measurements of black carbon aerosols over western trans-Himalayas: Seasonal heterogeneity and source apportionment, *J. Geophys. Res.*, *116*, D24201, doi:10.1029/2011JD016722.

Babu, S. S., and K. K. Moorthy (2002), Aerosol black carbon over a tropical coastal station in India, *Geophys. Res. Lett.*, *29*(23), 13-11–13-14, doi:10.1029/2002GL015662.

Beegum, S. N., et al. (2009), Spatial distribution of aerosol black carbon over India during pre-monsoon season, *Atmos. Environ.*, *43*(5), 1071–1078, doi:10.1016/j.atmosenv.2008.11.042.

Begum, B. A., A. Hossain, N. Nahar, A. Markwitz, and P. K. Hopke (2012), Organic and black carbon in $PM_{2.5}$ at an urban site at Dhaka, Bangladesh, *Aerosol Air Qual. Res.*, *12*(6), 1062–1072, doi:10.4209/aaqr.2012.05.0138.

Bonasoni, P., P. Laj, F. Angelini, J. Arduini, U. Bonafe, F. Calzolari, P. Cristofanelli, S. Decesari, M. Facchini, and S. Fuzzi (2008), The ABC-Pyramid Atmospheric Research Observatory in Himalaya for aerosol, ozone and halocarbon measurements, *Sci. Total Environ.*, *391*(2), 252–261.

Bond, T. C., E. Bhardwaj, R. Dong, R. Jogani, S. Jung, C. Roden, D. G. Streets, and N. M. Trautmann (2007), Historical emissions of black and organic carbon aerosol from energy-related combustion, 1850–2000, *Global Biogeochem. Cycles*, *21*, GB2018, doi:10.1029/2006GB002840.

Bond, T. C., et al. (2013), Bounding the role of black carbon in the climate system: A scientific assessment, *J. Geophys. Res. Atmos.*, *118*, 5380–5552, doi:10.1002/jgrd.50171.

Bond, T. C., G. Habib, and R. W. Bergstrom (2006), Limitations in the enhancement of visible light absorption due to mixing state, *J. Geophys. Res.*, *111*, D20211, doi:10.1029/2006JD007315.

Cao, J., S. F. Lee, K. Ho, X. Zhang, S. Zou, K. Fung, J. C. Chow, and J. G. Watson (2003), Characteristics of carbonaceous aerosol in Pearl River Delta Region, China during 2001 winter period, *Atmos. Environ.*, *37*(11), 1451–1460.

Cao, J. J., X. X. Tie, B. Q. Xu, Z. Z. Zhao, C. S. Zhu, G. H. Li, and S. X. Liu (2010), Measuring and modeling black carbon (BC) contamination in the SE Tibetan Plateau, *J. Atmos. Chem.*, *67*, 45–60.

Cao, J. J., C. S. Zhu, K. F. Ho, Y. M. Han, Z. X. Shen, C. L. Zhan, and J. Q. Zhang (2015), Light attenuation cross-section of black carbon in an urban atmosphere in northern China, *Particuology*, *18*, 89–95, doi:10.1016/j.partic.2014.04.011.

Chaubey, J. P., K. Krishna Moorthy, S. Suresh Babu, and V. S. Nair (2011), The optical and physical properties of atmospheric aerosols over the Indian Antarctic stations during southern hemispheric summer of the International Polar Year 2007–2008, *Ann. Geophys.*, *29*(1), 109–121, doi:10.5194/angeo-29-109-2011.

Chen, Y., J. J. Cao, J. Zhao, H. M. Xu, R. Arimoto, G. H. Wang, Y. M. Han, Z. X. Shen, and G. H. Li (2014), *n*-Alkanes and polycyclic aromatic hydrocarbons in total suspended particulates from the southeastern Tibetan Plateau: Concentrations, seasonal variations, and sources, *Sci. Total Environ.*, *470*, 9–18, doi:10.1016/j.scitotenv.2013.09.033.

Cheng, Y., et al. (2011), Mass absorption efficiency of elemental carbon and water-soluble organic carbon in Beijing, China, *Atmos. Chem. Phys.*, *11*(22), 11497–11510, doi:10.5194/acp-11-11497-2011.

Chow, J. C., J. G. Watson, L. W. A. Chen, M. C. O. Chang, N. F. Robinson, D. Trimble, and S. Kohl (2007), The IMPROVE_A temperature protocol for thermal/optical carbon analysis: Maintaining consistency with a long-term database, *J. Air Waste Manage. Assoc.*, *57*(9), 1014–1023, doi:10.3155/1047-3289.57.9.1014.

Cong, Z., S. Kang, X. Liu, and G. Wang (2007), Elemental composition of aerosol in the Nam Co region, Tibetan Plateau, during summer monsoon season, *Atmos. Environ.*, *41*(6), 1180–1187, doi:10.1016/j.atmosenv.2006.09.046.

Cong, Z., S. Kang, K. Kawamura, B. Liu, X. Wan, Z. Wang, S. Gao, and P. Fu (2015), Carbonaceous aerosols on the south edge of the Tibetan Plateau: Concentrations, seasonality and sources, *Atmos. Chem. Phys.*, *15*(3), 1573–1584, doi:10.5194/acp-15-1573-2015.

Dumka, U. C., K. K. Moorthy, R. Kumar, P. Hegde, R. Sagar, P. Pant, N. Singh, and S. S. Babu (2010), Characteristics of aerosol black carbon mass concentration over a high altitude location in the Central Himalayas from multi-year measurements, *Atmos. Res.*, *96*(4), 510–521, doi:10.1016/j.atmosres.2009.12.010.

Engling, G., Y. Zhang, C. Chan, X. F. Sang, M. Lin, K. Ho, Y. Li, C. Lin, and J. J. Lee (2011), Characterization and sources of aerosol particles over the southeastern Tibetan Plateau during the Southeast Asia biomass-burning season, *Tellus B*, *63*(1), 117–128.

Flanner, M. G., C. S. Zender, P. G. Hess, N. M. Mahowald, T. H. Painter, V. Ramanathan, and P. J. Rasch (2009), Springtime warming and reduced snow cover from carbonaceous particles, *Atmos. Chem. Phys.*, *9*(7), 2481–2497, doi:10.5194/acp-9-2481-2009.

Gadde, B., S. Bonnet, C. Menke, and S. Garivait (2009), Air pollutant emissions from rice straw open field burning in India, Thailand and the Philippines, *Environ. Pollut.*, *157*(5), 1554–1558, doi:10.1016/j.envpol.2009.01.004.

Gao, R. X., S. J. Niu, H. Zhang, J. Guo, D. M. Meng, J. H. Ma, J. H. Feng, and Y. J. Zhang (2007), A comparative study on black carbon aerosol observations in regions of Beijing and Lhasa in 2006, in *Proc. SPIE, Remote Sensing and Modeling of Ecosystems for Sustainability IV*, vol. 6679, 8 pp., San Diego, Calif., doi:10.1117/12.763956.

Gogoi, M. M., K. K. Moorthy, S. S. Babu, and P. K. Bhuyan (2009), Climatology of columnar aerosol properties and the influence of synoptic conditions: First-time results from the northeastern region of India, *J. Geophys. Res.*, *114*, D08202, doi:10.1029/2008JD010765.

Guleria, R. P., J. C. Kuniyal, P. P. Dhyani, R. Joshi, and N. L. Sharma (2014), Impact of aerosol on surface reaching solar irradiance over Mohal in the northwestern Himalaya, India, *J. Atmos. Sol. Terr. Phys.*, *108*, 41–49, doi:10.1016/j.jastp.2013.12.002.

Guo, S., M. Hu, Y. Lin, M. Gomez-Hernandez, M. L. Zamora, J. Peng, D. R. Collins, and R. Zhang (2016), OH-initiated oxidation of m-xylene on black carbon aging, *Environ. Sci. Technol.*, *50*(16), 8605–8612, doi:10.1021/acs.est.6b01272.

Haywood, J. M., and K. P. Shine (1997), Multi-spectral calculations of the direct radiative forcing of tropospheric sulphate and soot aerosols using a column model, *Q. J. R. Meteorol. Soc.*, *123*(543), 1907–1930, doi:10.1002/qj.49712354307.

Hess, M., P. Koepke, and I. Schult (1998), Optical Properties of Aerosols and Clouds: The software package OPAC, *Bull. Am. Meteorol. Soc.*, *79*(5), 831–844.

Hindman, E. E., and B. P. Upadhyay (2002), Air pollution transport in the Himalayas of Nepal and Tibet during the 1995–1996 dry season, *Atmos. Environ.*, *36*(4), 727–739.

Ho, S. S. H., J. C. Chow, J. G. Watson, L. P. Ting Ng, Y. Kwok, K. F. Ho, and J. Cao (2011), Precautions for in-injection port thermal desorption-gas chromatography/mass spectrometry (TD-GC/MS) as applied to aerosol filter samples, *Atmos. Environ.*, *45*(7), 1491–1496.

Hyvärinen, A. P., H. Lihavainen, M. Komppula, V. P. Sharma, V. M. Kerminen, T. S. Panwar, and Y. Viisanen (2009), Continuous measurements of optical properties of atmospheric aerosols in Mukteshwar, northern India, *J. Geophys. Res.*, *114*, D08207, doi:10.1029/2008JD011489.

Intergovernmental Panel on Climate Change (2013), in *Climate Change 2013: The Physical Science Basis. Contribution of Working Group I to the Fifth Assessment Report of the Intergovernmental Panel on Climate Change*, chap. 7, edited by T. F. Stocker et al., Cambridge Univ. Press, Cambridge, U. K.

Jacobson, M. Z. (2001), Strong radiative heating due to the mixing state of black carbon in atmospheric aerosols, *Nature*, *409*, 695–697.

Jacobson, M. Z. (2004), Climate response of fossil fuel and biofuel soot, accounting for soot's feedback to snow and sea ice albedo and emissivity, *J. Geophys. Res.*, *109*, D21201, doi:10.1029/2004JD004945.

Khalizov, A. F., Y. Lin, C. Qiu, S. Guo, D. Collins, and R. Zhang (2013), Role of OH-initiated oxidation of isoprene in aging of combustion soot, *Environ. Sci. Technol.*, *47*(5), 2254–2263, doi:10.1021/es3045339.

Khalizov, A. F., H. Xue, L. Wang, J. Zheng, and R. Zhang (2009), Enhanced light absorption and scattering by carbon soot aerosol internally mixed with sulfuric acid, *J. Phys. Chem. A*, *113*(6), 1066–1074, doi:10.1021/jp807531n.

Knox, A., G. J. Evans, J. R. Brook, X. Yao, C. H. Jeong, K. J. Godri, K. Sabaliauskas, and J. G. Slowik (2009), Mass absorption cross-section of ambient black carbon aerosol in relation to chemical age, *Aerosol Sci. Technol.*, *43*(6), 522–532, doi:10.1080/02786820902777207.

Kopacz, M., D. L. Mauzerall, J. Wang, E. M. Leibensperger, D. K. Henze, and K. Singh (2011), Origin and radiative forcing of black carbon transported to the Himalayas and Tibetan Plateau, *Atmos. Chem. Phys.*, *11*(6), 2837–2852.

Kulkarni, A. V. (2006), Glacial retreat in Himalaya using Indian remote sensing satellite data.

Lau, W. K., M.-K. Kim, K.-M. Kim, and W.-S. Lee (2010), Enhanced surface warming and accelerated snow melt in the Himalayas and Tibetan Plateau induced by absorbing aerosols, *Environ. Res. Lett.*, *5*(2), 025204.

Liu, S., et al. (2015), Enhanced light absorption by mixed source black and brown carbon particles in UK winter, *Nat. Commun.*, *6*, doi:10.1038/ncomms9435.

Madronich, S. (1993), UV radiation in the natural and perturbed atmosphere, in *Environmental Effects of UV (Ultraviolet) Radiation*, edited by M. Tevini, pp. 17–69, Lewis Publisher, Boca Raton, Fla.

Marcq, S., P. Laj, J. C. Roger, P. Villani, K. Sellegri, P. Bonasoni, A. Marinoni, P. Cristofanelli, G. P. Verza, and M. Bergin (2010), Aerosol optical properties and radiative forcing in the high Himalaya based on measurements at the Nepal Climate Observatory-Pyramid site (5079 m a.s.l.), *Atmos. Chem. Phys.*, *10*, 5859–5872.

Marinoni, A., P. Cristofanelli, P. Laj, R. Duchi, F. Calzolari, S. Decesari, K. Sellegri, E. Vuillermoz, G. Verza, and P. Villani (2010), Aerosol mass and black carbon concentrations, a two year record at NCO-P (5079 m, Southern Himalayas), *Atmos. Chem. Phys.*, *10*(17), 8551–8562.

Meehl, G. A., J. M. Arblaster, and W. D. Collins (2008), Effects of black carbon aerosols on the Indian monsoon, *J. Clim.*, *21*(12), 2869–2882, doi:10.1175/2007JCLI1777.1.

Ming, J., C. Xiao, H. Cachier, D. Qin, X. Qin, Z. Li, and J. Pu (2009), Black carbon (BC) in the snow of glaciers in west China and its potential effects on albedos, *Atmos. Res.*, *92*(1), 114–123, doi:10.1016/j.atmosres.2008.09.007.

Ming, J., C. Xiao, J. Sun, S. Kang, and P. Bonasoni (2010), Carbonaceous particles in the atmosphere and precipitation of the Nam Co region, central Tibet, *J. Environ. Sci.*, *22*(11), 1748–1756, doi:10.1016/s1001-0742(09)60315-6.

Nair, V. S., et al. (2007), Wintertime aerosol characteristics over the Indo-Gangetic Plain (IGP): Impacts of local boundary layer processes and long-range transport, *J. Geophys. Res.*, *112*, D13205, doi:10.1029/2006JD008099.

Oliveira, C., N. Martins, J. Tavares, C. Pio, M. Cerqueira, M. Matos, H. Silva, C. Oliveira, and F. Camões (2011), Size distribution of polycyclic aromatic hydrocarbons in a roadway tunnel in Lisbon, Portugal, *Chemosphere*, *83*(11), 1588–1596.

Peng, J., et al. (2016), Markedly enhanced absorption and direct radiative forcing of black carbon under polluted urban environments, *Proc. Natl. Acad. Sci. U.S.A.*, *113*(16), 4266–4271, doi:10.1073/pnas.1602310113.

Petzold, A., H. Schloesser, P. J. Sheridan, W. P. Arnott, J. A. Ogren, and A. Virkkula (2005), Evaluation of multiangle absorption photometry for measuring aerosol light absorption, *Aerosol Sci. Technol.*, *39*(1), 40–51, doi:10.1080/027868290901945.

Rai, K., A. K. Sarkar, and A. P. Mitra (2002), Chemical characterization of aerosols at NPL, Delhi, *IASTA Bull. Spec. Issue*, *14*(1), 155–158.

Raju, M. P., P. D. Safai, K. Vijayakumar, P. C. S. Devara, C. V. Naidu, P. S. P. Rao, and G. Pandithurai (2016), Atmospheric abundances of black carbon aerosols and their radiative impact over an urban and a rural site in SW India, *Atmos. Environ.*, *125*, 429–436, doi:10.1016/j.atmosenv.2015.09.023.

Ram, K., and M. M. Sarin (2009), Absorption coefficient and site-specific mass absorption efficiency of elemental carbon in aerosols from urban, rural and high-altitude sites in India, *Environ. Sci. Technol.*, *43*, 8233–8239.

Ram, K., M. M. Sarin, and P. Hegde (2008), Atmospheric abundances of primary and secondary carbonaceous species at two high-altitude sites in India: Sources and temporal variability, *Atmos. Environ.*, *42*(28), 6785–6796, doi:10.1016/j.atmosenv.2008.05.031.

Ram, K., M. M. Sarin, and P. Hegde (2010), Long-term record of aerosol optical properties and chemical composition from a high-altitude site (Manora Peak) in Central Himalaya, *Atmos. Chem. Phys.*, *10*(23), 11,791–11,803, doi:10.5194/acp-10-11791-2010.

Ramachandran, S., and T. A. Rajesh (2007), Black carbon aerosol mass concentrations over Ahmedabad, an urban location in western India: Comparison with urban sites in Asia, Europe, Canada, and the United States, *J. Geophys. Res.*, *112*, D06211, doi:10.1029/2006JD007488.

Ramanathan, V., et al. (2007), Atmospheric brown clouds: Hemispherical and regional variations in long-range transport, absorption, and radiative forcing, *J. Geophys. Res.*, *112*, D22S21, doi:10.1029/2006JD008124.

Safai, P. D., M. P. Raju, K. B. Budhavant, P. S. P. Rao, and P. C. S. Devara (2013), Long term studies on characteristics of black carbon aerosols over a tropical urban station Pune, India, *Atmos. Res.*, *132–133*, 173–184, doi:10.1016/j.atmosres.2013.05.002.

Schnaiter, M., H. Horvath, O. Möhler, K. H. Naumann, H. Saathoff, and O. W. Schöck (2003), UV-VIS-NIR spectral optical properties of soot and soot-containing aerosols, *J. Aerosol Sci.*, *34*(10), 1421–1444, doi:10.1016/S0021-8502(03)00361-6.

Schnaiter, M., C. Linke, O. Möhler, K. H. Naumann, H. Saathoff, R. Wagner, U. Schurath, and B. Wehner (2005), Absorption amplification of black carbon internally mixed with secondary organic aerosol, *J. Geophys. Res.*, *110*, D19204, doi:10.1029/2005JD006046.

Sheesley, R. J., J. J. Schauer, Z. Chowdhury, G. R. Cass, and B. R. T. Simoneit (2003), Characterization of organic aerosols emitted from the combustion of biomass indigenous to South Asia, *J. Geophys. Res.*, *108*(D9), 4285, doi:10.1029/2002JD002981.

Shiraiwa, M., Y. Kondo, N. Moteki, N. Takegawa, Y. Miyazaki, and D. R. Blake (2007), Evolution of mixing state of black carbon in polluted air from Tokyo, *Geophys. Res. Lett.*, *34*, L16803, doi:10.1029/2007GL029819.

Singh, S., S. Tiwari, D. P. Gond, U. C. Dumka, D. S. Bisht, S. Tiwari, G. Pandithurai, and A. Sinha (2015), Intra-seasonal variability of black carbon aerosols over a coal field area at Dhanbad, India, *Atmos. Res.*, *161–162*, 25–35, doi:10.1016/j.atmosres.2015.03.015.

Srivastava, A. K., K. Ram, P. Pant, P. Hegde, and J. Hema (2012), Black carbon aerosols over Manora Peak in the Indian Himalayan foothills: Implications for climate forcing, *Environ. Res. Lett.*, *7*(1), 014002.

Stohl, A., et al. (2006), Pan-Arctic enhancements of light absorbing aerosol concentrations due to North American boreal forest fires during summer 2004, *J. Geophys. Res.*, *111*, D22214, doi:10.1029/2006JD007216.
Stone, E. A., J. J. Schauer, B. B. Pradhan, P. M. Dangol, G. Habib, C. Venkataraman, and V. Ramanathan (2010), Characterization of emissions from South Asian biofuels and application to source apportionment of carbonaceous aerosol in the Himalayas, *J. Geophys. Res.*, *115*, doi:10.1029/2009JD011881.
Streets, D. G., et al. (2003), An inventory of gaseous and primary aerosol emissions in Asia in the year 2000, *J. Geophys. Res.*, *108*(D21), 8809, doi:10.1029/2002JD003093.
Stull, R. B. (1988), *An Introduction to Boundary Layer Meteorology*, chap. 1, Kluwer Acad., Dordrecht, Netherlands.
Tomasi, C., et al. (2007), Aerosols in polar regions: A historical overview based on optical depth and in situ observations, *J. Geophys. Res.*, *112*, D16205, doi:10.1029/2007JD008432.
Ueno, K., K. Toyotsu, L. Bertolani, and G. Tartari (2008), Stepwise onset of monsoon weather observed in the Nepal Himalayas, *Mon. Weather Rev.*, *136*(7), 2507–2522.
Venzac, H., et al. (2008), High frequency new particle formation in the Himalayas, *Proc. Natl. Acad. Sci. U.S.A.*, *105*(41), 15666–15671, doi:10.1073/pnas.0801355105.
Virkkula, A., T. Mäkelä, R. Hillamo, T. Yli-Tuomi, A. Hirsikko, K. Hämeri, and I. K. Koponen (2007), A simple procedure for correcting loading effects of aethalometer data, *J. Air Waste Manage. Assoc.*, *57*(10), 1214–1222, doi:10.3155/1047-3289.57.10.1214.
Wan, X., S. Kang, Y. Wang, J. Xin, B. Liu, Y. Guo, T. Wen, G. Zhang, and Z. Cong (2015), Size distribution of carbonaceous aerosols at a high-altitude site on the central Tibetan Plateau (Nam Co Station, 4730 m a.s.l.), *Atmos. Res.*, *153*, 155–164, doi:10.1016/j.atmosres.2014.08.008.
Wang, M., B. Q. Xu, N. L. Wang, J. J. Cao, X. X. Tie, H. L. Wang, C. S. Zhu, and W. Yang (2016), Two distinct patterns of seasonal variation of airborne black carbon over Tibetan Plateau, *Sci. Total Environ.*, *573*, 1041–1052, doi:10.1016/j.scitotenv.2016.08.184.
Wang, Q. Y., et al. (2015), Black carbon aerosol in winter northeastern Qinghai-Tibetan Plateau, China: The source, mixing state and optical property, *Atmos. Chem. Phys.*, *15*(22), 13059–13069, doi:10.5194/acp-15-13059-2015.
Weingartner, E., H. Saathoff, M. Schnaiter, N. Streit, B. Bitnar, and U. Baltensperger (2003), Absorption of light by soot particles: Determination of the absorption coefficient by means of aethalometers, *J. Aerosol Sci.*, *34*(10), 1445–1463, doi:10.1016/S0021-8502(03)00359-8.
Xia, X., X. Zong, Z. Cong, H. Chen, S. Kang, and P. Wang (2011), Baseline continental aerosol over the central Tibetan Plateau and a case study of aerosol transport from South Asia, *Atmos. Environ.*, *45*(39), 7370–7378, doi:10.1016/j.atmosenv.2011.07.067.
Xu, B. Q., et al. (2009), Black soot and the survival of Tibetan glaciers, *Proc. Natl. Acad. Sci. U.S.A.*, *106*(52), 22114–22118, doi:10.1073/pnas.0910444106.
Xu, J. Z., Z. B. Wang, G. M. Yu, X. Qin, J. W. Ren, and D. H. Qin (2014), Characteristics of water soluble ionic species in fine particles from a high altitude site on the northern boundary of Tibetan Plateau: Mixture of mineral dust and anthropogenic aerosol, *Atmos. Res.*, *143*(0), 43–56, doi:10.1016/j.atmosres.2014.01.018.
Zhang, R., A. F. Khalizov, J. Pagels, D. Zhang, H. Xue, and P. H. McMurry (2008), Variability in morphology, hygroscopicity, and optical properties of soot aerosols during atmospheric processing, *Proc. Natl. Acad. Sci. U.S.A.*, *105*(30), 10,291–10,296, doi:10.1073/pnas.0804860105.
Zhang, T., J. Cao, X. Tie, Z. Shen, S. Liu, H. Ding, Y. Han, G. Wang, K. Ho, and J. Qiang (2011), Water-soluble ions in atmospheric aerosols measured in Xi'an, China: Seasonal variations and sources, *Atmos. Res.*, *102*, 110–119.
Zhao, S., J. Ming, C. Xiao, W. Sun, and X. Qin (2012), A preliminary study on measurements of black carbon in the atmosphere of northwest Qilian Shan, *J. Environ. Sci.*, *24*(1), 152–159, doi:10.1016/S1001-0742(11)60739-0.
Zhao, Z., J. Cao, Z. Shen, B. Xu, C. Zhu, L. W. A. Chen, X. Su, S. Liu, Y. Han, and G. Wang (2013), Aerosol particles at a high-altitude site on the Southeast Tibetan Plateau, China: Implications for pollution transport from South Asia, *J. Geophys. Res. Atmos.*, *118*, 11360–11375.
Zhao, Z., J. Cao, Z. Shen, R.-J. Huang, T. Hu, P. Wang, T. Zhang, and S. Liu (2015), Chemical composition of PM2.5 at a high-altitude regional background site over Northeast of Tibet Plateau, *Atmos. Pollut. Res.*, *6*(5), 815–823, doi:10.5094/apr.2015.090.
Zhu, C., et al. (2016), Black carbon aerosols at Mt. Muztagh Ata, a high-altitude location in the western Tibetan Plateau, *Aerosol Air Qual. Res.*, *16*, 752–763.